Variable kinematic beam elements for electro-mechanical analysis

F. Miglioretti[*1], E. Carrera[1,2] and M. Petrolo[1]

[1]*Department of mechanical and aerospace engineering, Politecnico di Torino, Corso Duca degli Abruzzi, 24, 10129 Torino, Italy*
[2]*Faculty of Science, King Abdulaziz University, Jeddah 21589, Saudi Arabia*

Abstract.   This paper proposes a refined electro-mechanical beam formulation. Lagrange-type polynomials are used to interpolate the unknowns over the beam cross section. Three- (L3), four- (L4), and nine-point(L9) polynomials are considered which lead to linear, bi-linear, and quadratic displacement field approximations over the beam cross-section. Finite elements are obtained by employing the principle of virtual displacements in conjunction with the Carrera Unified Formulation (CUF). The finite element matrices and vectors are expressed in terms of fundamental nuclei whose forms do not depend on the assumptions made. Additional refined beam models are implemented by introducing further discretizations, over the beam cross-section. Some assessments from bibliography have been solved in order to validate the electro-mechanical formulation. The investigations conducted show that the present formulation is able to detect the electro-mechanical interaction.

Keywords: CUF; higher-order formulation; electro-mechanical formulation; finite elements

1. Introduction

Piezoelectric materials have the ability to convert mechanical energy into electrical energy, and vice versa. In 1880, Pierre and Jacques Curie discovered that certain crystals produce an electrical charge under deformation, where the amount of charge depends on the magnitude of the deformation. This effect is called the direct piezoelectric effect. The inverse effect, the so-called converse piezoelectric effect, was discovered by the Curie brothers in 1881, after Gabriel Lippman had deduced it on the basis of thermo dynamic principles. Through the converse effect, a crystal is deformed by means of an applied electric field. Renewed interest in this type of materials has emerged one the last twenty years. "Intelligent" or "smart structures" have been developed as a consequence of the progress that has been made in the field of composite multilayered structures and piezoelectric materials. There are various mathematical models in the bibliography that are able to describe the behaviour of piezoelectric structures. The strain induced by the piezoelectric actuators has been used in the works of Crawley and Luis (1987), Bailey and Hubbard (1985),and Robbins and Reddy(1991a) as an applied strain that contributes to the total strain of the non-active

---

∗Corresponding author, Dr., E-mail: federico.miglioretti@polito.it

structure. Crawley and Luis (1987) developed an analytical formulation that is able to model both surface bonded and embedded piezo-actuators in beams. For surface bonded actuators, they assumed a linear strain distribution in the beam substructures and a constant distribution in the actuator. For embedded actuators, they assumed a linear Euler-Bernulli-type strain distribution across the beam and the actuators. The work of Sarvanos and Heyliger (1999) offers a good review of the different theories, and classifies each work on the basis of the fundamental assumptions, the approximations of the through-the-thickness variation of the electro-mechanical state variables, the method of representation of the piezoelectric layers and the capability of modelling curvilinear geometries and thermal effects. In order to overcome the limitations of analytical formulations, many scientists have exploited finite element formulations to model composite piezoelectric structures. A few studies (Dong *et al.* (2006) and Xu and Koko (2004)) on the active vibration control of smart plates have been conducted using 3D solid-elements. The classical theory of smart beams and plates has been used to study the active vibration control of smart beams and plates by many researchers Kim and Kim (2005), Moitha *et al.* (2004) and Umesh and Ganguli (2009). The classical structural theory used in these studies is based on Kirchhoff-Love's assumptions and it neglects transverse shear deformation effects. A first-order shear deformation theory has been employed for the active vibration control of smart beams and plates by Caruso *et al.* (2003), Kumar and Narayanan (2007), Kusculuoglu and Royston (2005), Liu *et al.* (2004), Vasques and Rodrigues (2006). Although this theory includes the effects of transverse shear deformation, it requires a shear correction factor. The computation of such a correction factor is no easy for smart structures with arbitrary lay-outs. Zhou *et al.* (2000) have presented coupled finite element models based on a third-order theory for the dynamic response of smart composite plates. Carrera (1997) has developed a model for a multi-layered plate that include piezo-layers, which allows an accurate description of both the in-plane displacement (the zig-zag effect is included) and the transverse shear stress fields (interlaminar equilibrium is fulfilled). Moreover, it preserves the computational advantages of the standard Reissner-Mindlin finite element formulation. Electrical stiffnesses are taken into account by assuming aquadratic distribution along the thickness for the voltage field. Moita *et al.* (2005) have presented a single layer triangular nonconforming plate/shell element with 24 degrees of freedom for generalized displacements, and one electrical potential degree of freedom for each piezoelectric element layer based on a third-order sheared formation theory. Beheshti-Aval *et al.* (2011) have proposed a three-node beam finite element for the analysis of piezoelectric beams based on a refined sinus model, which does not require a shear correction factor. A higher-order electrical potential field was considered for each piezoelectric layer. Marinkovic *et al.* (2007) have proposed thin-walled active structures that utilize the piezoelectric patches as both sensor and actuator components. They developed a shell element that uses higher-order functions to model the electric quantities. Vidal *et al.* (2011) have presented a finite element for shell structures with piezoelectric actuators and sensors based on a conventional 8-node shell formulation and classical displacement theories. The element describes transverse kinematics in order to consistently retain full 3D piezoelectric coupling. A layer-wise description of the electric degree of freedom also permits one to account for embedded piezoelectric layers. Biscani *et al.* (2012) have proposed a finite element model for the coupling of piezoelectric plate elements based on different through-the-thickness expansions using the Arlequin method. The model was formulated on the basis of the Carrera unified formulation (CUF). The computational costs were reduced by assuming refined models only in those zones of the structure in which high accuracy was required. Ballhause *et al.* (2005) have proposed a unified formulation for the electro-mechanical analysis of multilayered plates embedding piezo-layers. Both equivalent single

layer (ESL) and layer-wise (LW) models were considered. Zig-zag effects were described by employing the Murakami zig-zag function. Linear and up to fourth-order expansions were used for displacement variables. Carrera and Boscolo (2006) have used the CUF and the Reissner mixed variational theorem (RMVT) to develop a finite element for the static and dynamic analysis of multilayered plates with embedded piezoelectric layers. The book by Carrera *et al.* (2011) presents a detailed analysis of classical and advanced structural models that are able to deal with mechanical and electric field loadings. Elshafei and Alraiess (2013) have developed a finite element formulation to model and analyse isotropic as well as orthotropic composite beams with distributed piezoelectric actuators subjected to both mechanical and electrical loads. The model was formulated on the basis of a simple higher-order shear deformation theory. The electric potential was considered as a function of the thickness and the length of the beam element. The present work falls in the frame of CUF, which was developed over the last decade. CUF is a hierarchical formulation that considers the order of the theory as an input of the analysis. Non-classical effects (e.g., warping, in-plane deformations, shear effects, bending-torsion coupling) are accounted for by opportunely increasing the order of the adopted model. In the works of Carrera *et al.* (2010), Carrera *et al.* (2011), Carrera *et al.* (2012a), Carrera *et al.* (2012b), the finite element formulation was adopted to deal with arbitrary geometries, boundary conditions and loadings. The displacement field above the cross-section was defined through Taylor-type polynomials. Static analyses (Carrera *et al.* (2010), Carrera *et al.* (2011)) have shown that the CUF is able to capture warping, in-plane deformations and shear effects. Free vibration analyses (Carrera *et al.* (2012a), Carrera *et al.* (2012b)) have underlined the possibility of detecting shell-like vibration modes. In the work of Carrera and Petrolo (2012), the displacement field above the cross-section has been described using Lagrange-type polynomials. The variables for this kind of expansion functions acquire a precise physical meaning. In the work of Carrera and Petrolo (2012), the choice of Lagrange-type polynomials has led to having only pure displacement variables. A multi-field beam formulation based on the Carrera Unified Formulations is proposed in this work . The unknowns above the cross-section are described by Lagrange-type polynomials. The problem unknowns for the electro-mechanical formulation are the translational displacements (u_x, u_y, u_z) and the electrical potential (φ). Three- (L3), four- (L4), and nine-point (L9) polynomials are considered in the framework of CUF; this leads to linear, bi-linear, and quadratic unknown fields. More refined beam models are implemented by introducing further discretizations over the beam cross-section. This paper is organized as follows: a description of the electro-mechanical constitutive equations is provided in Section 2. A brief description of the adopted beam theories and finite element formulations is provided in Section 3. The results are presented in Section 4.

2. Preliminaries

The coordinate reference frame is shown in Fig. 1. In Fig. 2, the material coordinate system and the problem coordinate system are indicated for a laminate. The single subscript notation for stress and strain components is based on the following convention

$$\sigma_1 = \sigma_{11}, \sigma_2 = \sigma_{22}, \sigma_3 = \sigma_{33}, \sigma_4 = \sigma_{12}, \sigma_5 = \sigma_{13}, \sigma_6 = \sigma_{23}$$

$$\epsilon_1 = \epsilon_{11}, \epsilon_2 = \epsilon_{22}, \epsilon_3 = \epsilon_{33}, \epsilon_4 = \epsilon_{12}, \epsilon_5 = \epsilon_{13}, \epsilon_6 = \epsilon_{23}$$

(1)

In the pure mechanical cases, the stress, σ, and strain, ϵ, components are grouped as

$$\boldsymbol{\sigma} = \left\{\sigma_{xx}, \sigma_{yy}, \sigma_{zz}, \sigma_{yz}, \sigma_{xz}, \sigma_{xy},\right\}^T$$

$$\boldsymbol{\epsilon} = \left\{\epsilon_{xx}, \epsilon_{yy}, \epsilon_{zz}, \epsilon_{yz}, \epsilon_{xz}, \epsilon_{xy},\right\}^T$$

(2)

and they are related via Hook's law

$$\boldsymbol{\sigma} = \widetilde{\boldsymbol{C}} \, \boldsymbol{\epsilon}$$

(3)

where $\widetilde{\boldsymbol{C}}$ is the Hooke law stiffness matrix in the problem reference system

$$\begin{Bmatrix} \sigma_{xx} \\ \sigma_{yy} \\ \sigma_{zz} \\ \sigma_{yz} \\ \sigma_{xz} \\ \sigma_{xy} \end{Bmatrix} = \begin{bmatrix} \tilde{C}_{22} & \tilde{C}_{23} & \tilde{C}_{21} & 0 & 0 & \tilde{C}_{26} \\ \tilde{C}_{32} & \tilde{C}_{33} & \tilde{C}_{31} & 0 & 0 & \tilde{C}_{36} \\ \tilde{C}_{12} & \tilde{C}_{13} & \tilde{C}_{11} & 0 & 0 & \tilde{C}_{16} \\ 0 & 0 & 0 & \tilde{C}_{55} & \tilde{C}_{54} & 0 \\ 0 & 0 & 0 & \tilde{C}_{45} & \tilde{C}_{44} & 0 \\ \tilde{C}_{62} & \tilde{C}_{63} & \tilde{C}_{61} & 0 & 0 & \tilde{C}_{66} \end{bmatrix} \begin{Bmatrix} \epsilon_{xx} \\ \epsilon_{yy} \\ \epsilon_{zz} \\ \epsilon_{yz} \\ \epsilon_{xz} \\ \epsilon_{xy} \end{Bmatrix}$$

(4)

The electric problem can be described through the electric field strength E and the dielectric displacement D. In Fig. 3, the polarization axes and the external polarization field used to build the piezo-material are reported. The electrical properties of the piezo-material are expressed according to the polarization axes in Fig. 3,

$$\boldsymbol{D}_e^T = \{D_1, D_2, D_3\} \boldsymbol{E}^T = \{E_1, E_2, E_3\}$$

(5)

Their relation in the uncoupled case is

$$\boldsymbol{D}_e = \boldsymbol{\chi} \boldsymbol{E}$$

(6)

where $\boldsymbol{\chi}$ is the dielectric permittivity matrix of the materials

$$\boldsymbol{\chi} = \begin{bmatrix} \chi_{11} & \chi_{12} & 0 \\ \chi_{21} & \chi_{22} & 0 \\ 0 & 0 & \chi_{33} \end{bmatrix}$$

(7)

In the case of piezoelectric materials, the mechanical and the electrical systems are coupled. Therefore the two uncoupled constitutive Eqs. (3) and (6) have to be extended with coupling terms. The coupled constitutive equations can take different forms, depending on the used combinations of the variables. The strains can be expressed in terms of the electric field and the dielectric displacements in terms of the stresses using the piezoelectric coefficients d. This formulation is called d−form

$$\boldsymbol{\epsilon} = \tilde{\boldsymbol{S}} \boldsymbol{\sigma} - \boldsymbol{d}^T \boldsymbol{E}$$

$$\boldsymbol{D}_e = \boldsymbol{d} \boldsymbol{\sigma} + \boldsymbol{\chi} \boldsymbol{E}$$

(8)

where $\tilde{\boldsymbol{S}}$ is the compliance matrix, which is the inverse of the elasticity matrix $\tilde{\boldsymbol{S}} = \widetilde{\boldsymbol{C}}^{-1}$ and $\boldsymbol{d}$ is

$$\boldsymbol{d} = \begin{bmatrix} 0 & 0 & 0 & d_{15} & 0 & 0 \\ 0 & 0 & 0 & 0 & d_{24} & 0 \\ d_{32} & d_{33} & d_{31} & 0 & 0 & 0 \end{bmatrix}$$

(9)
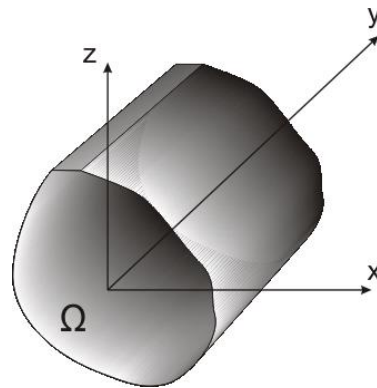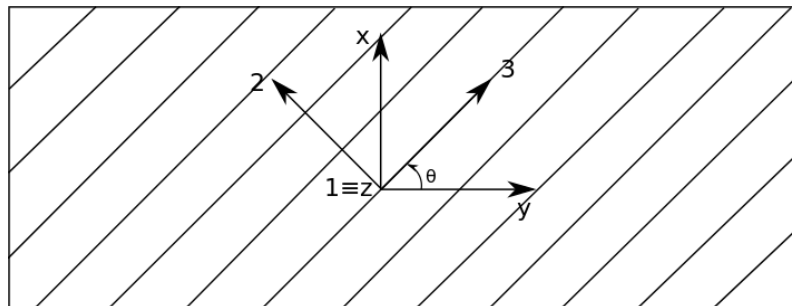
Fig. 1 Reference system

Fig. 2 Fibre orientation angle

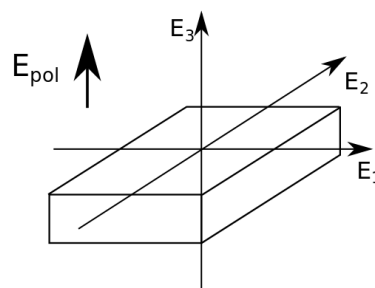

Fig. 3 Polarization Axes

The most adopted formulation is the so called e-form, which relates the mechanical stresses to the electric field and the dielectric displacements to the mechanical strains via the piezoelectric stiffness coefficients e

$$\sigma = \tilde{C}\epsilon - e^T E$$

$$D_e = e\epsilon + \chi E \tag{10}$$

The piezoelectric coefficient matrix d and the piezoelectric stiffness matrix e have following relation

$$e^T = \tilde{C}d^T \tag{11}$$

The matrix e is

$$e = \begin{bmatrix} 0 & 0 & 0 & e_{15} & e_{14} & 0 \\ 0 & 0 & 0 & e_{25} & e_{24} & 0 \\ e_{32} & e_{33} & e_{31} & 0 & 0 & e_{36} \end{bmatrix} \tag{12}$$

where

$$\begin{aligned}
e_{32} &= d_{32}\tilde{C}_{22} + d_{33}\tilde{C}_{23} + d_{31}\tilde{C}_{21} \\
e_{33} &= d_{32}\tilde{C}_{32} + d_{33}\tilde{C}_{33} + d_{31}\tilde{C}_{31} \\
e_{31} &= d_{32}\tilde{C}_{12} + d_{33}\tilde{C}_{13} + d_{31}\tilde{C}_{11} \\
e_{36} &= d_{32}\tilde{C}_{26} + d_{33}\tilde{C}_{36} + d_{31}\tilde{C}_{16} \\
e_{14} &= d_{15}\tilde{C}_{45}e_{24} = d_{24}\tilde{C}_{44} \\
e_{15} &= d_{15}\tilde{C}_{55}e_{25} = d_{24}\tilde{C}_{54}
\end{aligned} \tag{13}$$

In this work the $e-$form (Eq. (10)) has been adopted. By mixing together the strain and stress matrices (Eq. (2)) with the electric field and electric displacement matrices (Eq. (5)) it is possible to write the constitutive equations in a compact manner (it is necessary to change the sign in order to be coherent with the Eq. (10))

$$\bar{\sigma} = \tilde{H}\bar{\epsilon} \tag{14}$$

where

$$\bar{\sigma} = \{\sigma_{xx} \quad \sigma_{yy} \quad \sigma_{zz} \quad \sigma_{yz} \quad \sigma_{xz} \quad \sigma_{xy} \quad -D_1 \quad -D_2 \quad -D_2\}^T$$

$$\tag{15}$$

$$\bar{\epsilon} = \{\epsilon_{xx} \quad \epsilon_{yy} \quad \epsilon_{zz} \quad \epsilon_{yz} \quad \epsilon_{xz} \quad \epsilon_{xy} \quad E_1 \quad E_2 \quad E_3\}^T$$

and $\tilde{H}$ combine together mechanical constants, electrical constants and electro-mechanical constants

$$\tilde{H} = \begin{bmatrix} \tilde{C}_{22} & \tilde{C}_{23} & \tilde{C}_{21} & 0 & 0 & \tilde{C}_{26} & 0 & 0 & -e_{32} \\ \tilde{C}_{32} & \tilde{C}_{33} & \tilde{C}_{31} & 0 & 0 & \tilde{C}_{36} & 0 & 0 & -e_{33} \\ \tilde{C}_{12} & \tilde{C}_{13} & \tilde{C}_{11} & 0 & 0 & \tilde{C}_{16} & 0 & 0 & -e_{31} \\ 0 & 0 & 0 & \tilde{C}_{55} & \tilde{C}_{54} & 0 & -e_{15} & -e_{25} & 0 \\ 0 & 0 & 0 & \tilde{C}_{45} & \tilde{C}_{44} & 0 & -e_{14} & -e_{24} & 0 \\ \tilde{C}_{62} & \tilde{C}_{63} & \tilde{C}_{61} & 0 & 0 & \tilde{C}_{66} & 0 & 0 & -e_{36} \\ 0 & 0 & 0 & -e_{15} & -e_{14} & 0 & -\chi_{11} & -\chi_{12} & 0 \\ 0 & 0 & 0 & -e_{25} & -e_{24} & 0 & -\chi_{21} & -\chi_{22} & 0 \\ -e_{32} & -e_{33} & -e_{31} & 0 & 0 & -e_{36} & 0 & 0 & -\chi_{33} \end{bmatrix} \tag{16}$$

The strains and the electric field are obtained as

$$\bar{\epsilon} = D u \tag{17}$$

where

$$u = \{u_x \quad u_y \quad u_z \quad \phi\} \tag{18}$$

and

$$D = \begin{bmatrix} \delta_x & 0 & 0 & 0 \\ 0 & \delta_y & 0 & 0 \\ 0 & 0 & \delta_z & 0 \\ 0 & \delta_z & \delta_y & 0 \\ \delta_z & 0 & \delta_x & 0 \\ \delta_y & \delta_x & 0 & 0 \\ 0 & 0 & 0 & -\delta_x \\ 0 & 0 & 0 & -\delta_y \\ 0 & 0 & 0 & -\delta_z \end{bmatrix} \tag{19}$$

3. Unified FE formulation

In the framework of the unified formulation, the beam cross-section unknowns are described by an expansion of generic functions, F_τ

$$u = F_\tau u_\tau \tau = 1,2,\dots,M \tag{20}$$

where $F\tau$ are functions of the cross-section coordinates x and z, u_τ is the unknown vector and M standsfor the number of terms expansion. According to the Einstein notation, the repeated subscripted τ indicate summations. The choice of F_τ and M is arbitrary, that is, different cross-section functions of any-order can be taken into account to model the unknowns of a beam above the cross-section. Taylor-type expansions have been exploited in the works of Carrera and Giunta (2010), Carrera and Petrolo (2011), and Carrera *et al.* (2010), Carrera *et al.* (2011), Carrera *et al.* (2012a), Carrera *et al.* (2012b). The Euler-Bernoulli and Timoshenko classical theories are derived from the linear Taylor-type expansion. For the electromechanical problem the Lagrange polynomials are more convenient. Them are herein used to describe the cross-section unknowns. Three-,L3, four-,L4 and nine-,L9, polynomials are adopted. L3 polynomials are defined on a

triangular domain which is identified by three points. These points define the element that is used to model the displacement field above the cross-section. Similarly, L4 and L9 cross-section elements are defined on quadrilateral domains. The iso-parametric formulation is exploited. In the case of L3 elements, the interpolation functions are given by Onate (2009)

$$F_1 = 1 - r - s \quad F_2 = r \quad F_2 = s \tag{21}$$

where r and s belong to the triangular domain defined by the points in Table 1. Fig. 4(a) shows the point locations in actual coordinates. The L4 element interpolation functions are given by

$$F_\tau = \frac{1}{4}(1 + rr_\tau)(1 + ss_\tau) \quad \tau = 1,2,3,4 \tag{22}$$

where r and s vary from -1 to 1. Fig. 4(b) shows the point locations and Table 2 reports the point natural coordinates. In the case of an L9 element the interpolation functions are given by

$$F_\tau = \frac{1}{4}(r^2 + rr_\tau)(s^2 + ss_\tau) \quad \tau = 1,3,5,7$$

$$F_\tau = \frac{1}{2}s_\tau^2(s^2 + ss_\tau)(1 - r^2) + \frac{1}{2}r_\tau^2(r^2 + rr_\tau)(1 - s^2) \quad \tau = 2,4,6,8 \tag{23}$$
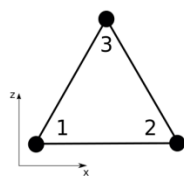
$$F_\tau = (1 - r^2)(1 - s^2) \quad \tau = 9$$

where r and s vary from 1 to $+1$. Fig. 4(c) shows the point locations and Table 3 reports the point natural coordinates. The cross-section unknowns given by an L4 element are

$$
\begin{aligned}
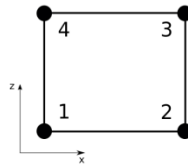u_x &= F_1 u_{x1} + F_2 u_{x2} + F_3 u_{x3} + F_4 u_{x4} \\
u_y &= F_1 u_{y1} + F_2 u_{y2} + F_3 u_{y3} + F_4 u_{y4} \\
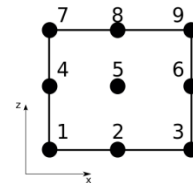u_z &= F_1 u_{z1} + F_2 u_{z2} + F_3 u_{z3} + F_4 u_{z4} \\
u_\phi &= F_1 u_{\phi1} + F_2 u_{\phi2} + F_3 u_{\phi3} + F_4 u_{\phi4}
\end{aligned}
\tag{24}
$$

(a) L3 element   (b) L4 element   (c) L9 element

Fig. 4 Cross-section elements

Table 1 L3 cross-section element point natural coordinates

Points	r	s
1	0	0
2	1	0
3	0	1

Table 2 L4 cross-section element point natural coordinates

Points	r	s
1	-1	-1
2	1	-1
3	1	1
4	-1	1

where $u_{x1}, \ldots, u_{z4}$ are the displacement variables and $\phi_1, \ldots, \phi_4$ are the voltage variables of the problem, and they represent the translational displacement components and the voltage components of each of the four points of the L4 element. The cross-section can be discretized by means of several L-elements. Fig. 5 shows the assembly of 2 L9 which share a common edge and three points. The discretization along the beam axis is conducted via a classical finite element approach. The unknown vector is given by

$$\boldsymbol{u} = N_i F_\tau \boldsymbol{q}_{\tau i} \tag{25}$$

where N_i stands for the shape functions and $\boldsymbol{q}_{\tau i}$ for the nodal unknown vector

$$\boldsymbol{q}_{\tau i} = \left\{ q_{ux_{\tau i}}, q_{uy_{\tau i}}, q_{uz_{\tau i}}, q_{\phi_{\tau i}} \right\} \tag{26}$$

For the sake of brevity, the shape functions are not reported here. They can be found in many books, for instance in Bathe (1996). Elements with four nodes (B4) are herein adopted, that is, a cubic approximation along the y axis is adopted. It has to be highlighted that the adopted cross-section displacement model defines the beam theory. It is therefore possible to deal with linear (L3), bilinear (L4) and quadratic (L9) beam theories. Further refinements can be obtained by adding cross-section elements in this case the beam model will be defined by the number of cross-section elements used. The choice of the cross-section discretization (that is the choice of the type, the number and the distribution of cross-section elements) is completely independent of the choice of the beam finite element to be used along the beam axis. The stiffness matrix of the elements and the external loadings, which are consistent with the model, are obtained via the Principle of Virtual Displacements

$$\delta L_{int} = \int_V (\delta \bar{\epsilon}^T \bar{\sigma}) dV = \delta L_{ext} \tag{27}$$

where L_{int} stands for the strain energy, L_{ext} is the work of the external loadings, and δ stands for the virtual variation. By introducing Eqs. (14), (17) and (25), Eq. (27) becomes

$$\delta L_{int} = \delta \boldsymbol{q}_{\tau i}^T \int_V (N_i \boldsymbol{I} F_\tau)^T \boldsymbol{D}^T \widetilde{\boldsymbol{H}} \boldsymbol{D} (N_j \boldsymbol{I} F_s) dV \, \boldsymbol{q}_{sj} = \delta L_{ext} \tag{28}$$

where

$$\boldsymbol{I} = \begin{bmatrix} 1 & 0 & 0 & 0 \\ 0 & 1 & 0 & 0 \\ 0 & 0 & 1 & 0 \\ 0 & 0 & 0 & 1 \end{bmatrix} \tag{29}$$
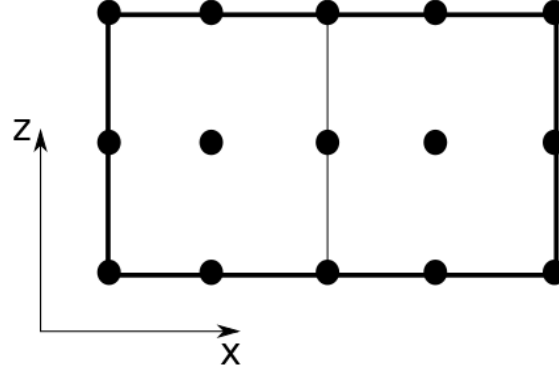
Fig. 5 Two assembled L9 elements

From Eq. (28), it is possible to obtain the stiffness matrix written in the form of the fundamental nuclei

$$\delta L_{int} = \delta \boldsymbol{q}_{\tau i}^{T} \boldsymbol{K}^{ij\tau s} \boldsymbol{q}_{sj} \tag{30}$$

The unified form of the virtual variation of the strain energy can be written as follows.

$$\boldsymbol{K}^{ij\tau s} = \int_{V} (N_i I F_{\tau})^{T} \boldsymbol{D}^{T} \widetilde{\boldsymbol{H}} \boldsymbol{D} (N_j I F_s) dV \tag{31}$$

Superscripts indicate the four indexes exploited to assemble the matrix: i and j are related to the shape functions, τ and s are related to the expansion functions. The components of the stiffness matrix are

$$
\begin{aligned}
K_{11}^{ij\tau s} =\ & \widetilde{C_{66}} \int_{\Omega} F_{\tau} F_{s} dxdz \int_{l} N_{i,y} N_{j,y} dy + \widetilde{C_{26}} \int_{\Omega} F_{\tau,x} F_{s} dxdz \int_{l} N_{i} N_{j,y} dy \\
& + \widetilde{C_{44}} \int_{\Omega} F_{\tau,z} F_{s,z} dxdz \int_{l} N_{i} N_{j} dy \\
& + \widetilde{C_{26}} \int_{\Omega} F_{\tau} F_{s,x} dxdz \int_{l} N_{i,y} N_{j} dy \\
& + \widetilde{C_{22}} \int_{\Omega} F_{\tau,x} F_{s,x} dxdz \int_{l} N_{i} N_{j} dy
\end{aligned}
\tag{32}
$$

$$K_{12}^{ij\tau s} = \widetilde{C_{66}} \int_\Omega F_\tau F_{s,x}\,dxdz \int_l N_{i,y}N_j\,dy + \widetilde{C_{26}} \int_\Omega F_{\tau,x}F_{s,x}\,dxdz \int_l N_i N_j\,dy$$

$$+ \widetilde{C_{45}} \int_\Omega F_{\tau,z}F_{s,z}\,dxdz \int_l N_i N_j\,dy$$

$$+ \widetilde{C_{36}} \int_\Omega F_\tau F_s\,dxdz \int_l N_{i,y}N_{j,y}\,dy$$

$$+ \widetilde{C_{23}} \int_\Omega F_{\tau,x}F_s\,dxdz \int_l N_i N_{j,y}\,dy$$

$$K_{13}^{ij\tau s} = \widetilde{C_{45}} \int_\Omega F_{\tau,z}F_s\,dxdz \int_l N_i N_{j,y}\,dy + \widetilde{C_{44}} \int_\Omega F_{\tau,z}F_{s,x}\,dxdz \int_l N_i N_j\,dy$$

$$+ \widetilde{C_{21}} \int_\Omega F_{\tau,x}F_{s,z}\,dxdz \int_l N_i N_j\,dy$$

$$+ \widetilde{C_{16}} \int_\Omega F_\tau F_{s,z}\,dxdz \int_l N_{i,y}N_j\,dy$$

$$K_{14}^{ij\tau s} = e_{14} \int_\Omega F_{\tau,z}F_{s,x}\,dxdz \int_l N_i N_j\,dy + e_{24} \int_\Omega F_{\tau,z}F_s\,dxdz \int_l N_i N_{j,y}\,dy$$

$$+ e_{31} \int_\Omega F_{\tau,x}F_{s,z}\,dxdz \int_l N_i N_j\,dy$$

$$+ e_{36} \int_\Omega F_\tau F_{s,z}\,dxdz \int_l N_{i,y}N_j\,dy$$

$$K_{22}^{ij\tau s} = \widetilde{C_{66}} \int_\Omega F_{\tau,x}F_{s,x}\,dxdz \int_l N_i N_j\,dy + \widetilde{C_{36}} \int_\Omega F_\tau F_{s,x}\,dxdz \int_l N_{i,y}N_j\,dy$$

$$+ \widetilde{C_{55}} \int_\Omega F_{\tau,z}F_{s,z}\,dxdz \int_l N_i N_j\,dy$$

$$+ \widetilde{C_{36}} \int_\Omega F_{\tau,x}F_s\,dxdz \int_l N_i N_{j,y}\,dy$$

$$+ \widetilde{C_{33}} \int_\Omega F_\tau F_s\,dxdz \int_l N_{i,y}N_{j,y}\,dy$$

$$K_{23}^{ij\tau s} = \widetilde{C_{55}} \int_\Omega F_{\tau,z}F_s\,dxdz \int_l N_i N_{j,y}\,dy + \widetilde{C_{45}} \int_\Omega F_{\tau,z}F_{s,x}\,dxdz \int_l N_i N_j\,dy$$

$$+ \widetilde{C_{16}} \int_\Omega F_{\tau,x}F_{s,z}\,dxdz \int_l N_i N_j\,dy$$

$$+ \widetilde{C_{13}} \int_\Omega F_\tau F_{s,z}\,dxdz \int_l N_{i,y}N_j\,dy$$

$$K_{24}^{ij\tau s} = e_{15} \int_{\Omega} F_{\tau,z} F_{s,x} dx dz \int_{l} N_i N_j dy + e_{25} \int_{\Omega} F_{\tau,z} F_s dx dz \int_{l} N_i N_{j,y} dy$$

$$+ e_{36} \int_{\Omega} F_{\tau,x} F_{s,z} dx dz \int_{l} N_i N_j dy$$

$$+ e_{32} \int_{\Omega} F_\tau F_{s,z} dx dz \int_{l} N_{i,y} N_j dy$$

$$K_{31}^{ij\tau s} = \widetilde{C_{45}} \int_{\Omega} F_\tau F_{s,z} dx dz \int_{l} N_{i,y} N_j dy + \widetilde{C_{44}} \int_{\Omega} F_{\tau,x} F_{s,z} dx dz \int_{l} N_i N_j dy$$

$$+ \widetilde{C_{16}} \int_{\Omega} F_{\tau,z} F_s dx dz \int_{l} N_i N_{j,y} dy$$

$$+ \widetilde{C_{12}} \int_{\Omega} F_{\tau,z} F_{s,x} dx dz \int_{l} N_i N_j dy$$

$$K_{32}^{ij\tau s} = \widetilde{C_{55}} \int_{\Omega} F_\tau F_{s,z} dx dz \int_{l} N_{i,y} N_j dy + \widetilde{C_{45}} \int_{\Omega} F_{\tau,x} F_{s,z} dx dz \int_{l} N_i N_j dy$$

$$+ \widetilde{C_{16}} \int_{\Omega} F_{\tau,z} F_{s,x} dx dz \int_{l} N_i N_j dy$$

$$+ \widetilde{C_{13}} \int_{\Omega} F_{\tau,z} F_s dx dz \int_{l} N_i N_{j,y} dy$$

$$K_{33}^{ij\tau s} = \widetilde{C_{55}} \int_{\Omega} F_\tau F_s dx dz \int_{l} N_{i,y} N_{j,y} dy + \widetilde{C_{45}} \int_{\Omega} F_{\tau,x} F_s dx dz \int_{l} N_i N_{j,y} dy$$

$$+ \widetilde{C_{45}} \int_{\Omega} F_\tau F_{s,x} dx dz \int_{l} N_{i,y} N_j dy$$

$$+ \widetilde{C_{44}} \int_{\Omega} F_{\tau,x} F_{s,x} dx dz \int_{l} N_i N_j dy$$

$$+ \widetilde{C_{11}} \int_{\Omega} F_{\tau,z} F_{s,z} dx dz \int_{l} N_i N_j dy$$

$$K_{34}^{ij\tau s} = e_{33} \int_{\Omega} F_{\tau,z} F_{s,z} dx dz \int_{l} N_i N_j dy + e_{24} \int_{\Omega} F_{\tau,x} F_s dx dz \int_{l} N_i N_{j,y} dy$$

$$+ e_{25} \int_{\Omega} F_\tau F_s dx dz \int_{l} N_{i,y} N_{j,y} dy$$

$$+ e_{14} \int_{\Omega} F_{\tau,x} F_{s,x} dx dz \int_{l} N_i N_j dy$$

$$+ e_{15} \int_{\Omega} F_\tau F_{s,x} dx dz \int_{l} N_{i,y} N_j dy$$

$$K_{41}^{ij\tau s} = e_{31} \int_{\Omega} F_{\tau,z} F_{s,x} dx dz \int_{l} N_i N_j dy + e_{36} \int_{\Omega} F_{\tau,z} F_s dx dz \int_{l} N_i N_{j,y} dy$$

$$+ e_{14} \int_{\Omega} F_{\tau,x} F_{s,z} dx dz \int_{l} N_i N_j dy$$

$$+ e_{24} \int_{\Omega} F_\tau F_{s,z} dx dz \int_{l} N_{i,y} N_j dy$$

$$K_{42}^{ij\tau s} = e_{36} \int_\Omega F_{\tau,z} F_{s,x} dxdz \int_l N_i N_j dy + e_{32} \int_\Omega F_{\tau,z} F_s dxdz \int_l N_i N_{j,y} dy$$

$$+ e_{15} \int_\Omega F_{\tau,x} F_{s,z} dxdz \int_l N_i N_j dy$$

$$+ e_{25} \int_\Omega F_\tau F_{s,z} dxdz \int_l N_{i,y} N_j dy$$

$$K_{43}^{ij\tau s} = e_{33} \int_\Omega F_{\tau,z} F_{s,z} dxdz \int_l N_i N_j dy + e_{15} \int_\Omega F_{\tau,x} F_s dxdz \int_l N_i N_{j,y} dy$$

$$+ e_{25} \int_\Omega F_\tau F_s dxdz \int_l N_{i,y} N_{j,y} dy$$

$$+ e_{14} \int_\Omega F_{\tau,x} F_{s,x} dxdz \int_l N_i N_j dy$$

$$+ e_{24} \int_\Omega F_\tau F_{s,x} dxdz \int_l N_{i,y} N_j dy$$

$$K_{44}^{ij\tau s} = -\chi_{33} \int_\Omega F_{\tau,z} F_{s,z} dxdz \int_l N_i N_j dy$$

$$- \chi_{22} \int_\Omega F_\tau F_s dxdz \int_l N_{i,y} N_{j,y} dy$$

$$- \chi_{12} \int_\Omega F_{\tau,x} F_s dxdz \int_l N_i N_{j,y} dy$$

$$- \chi_{12} \int_\Omega F_\tau F_{s,x} dxdz \int_l N_{i,y} N_j dy$$

$$- \chi_{11} \int_\Omega F_{\tau,x} F_{s,x} dxdz \int_l N_i N_j dy$$

The fundamental nucleus is a $4x4$ array which is formally independent of the order of the beam model and of the choice of the F_τ expansion polynomials.These are the key-points of CUF which permit, with only nine FORTRAN statements, to implement any-order theories. The assembly procedure of the stiffness matrix is based on the use of the four indexes τ, s, i and j which are opportunely exploited to implement the FORTRAN statements.

3.1 Mass matrix

The virtual variation of the work of the inertial loadings is

$$\delta L_{ine} = \int_v \rho \ddot{\boldsymbol{u}} \delta \boldsymbol{u}^T dV \tag{33}$$

where ρ stands for the density of the material, and $\ddot{\boldsymbol{u}}$ is the acceleration vector. Eq. (33) can be rewritten using Eqs. 17 and (25)

$$\delta L_{ine} = \delta \boldsymbol{q}_{\tau i}^T \int_v N_i (F_\tau \boldsymbol{I}) \rho (F_s \boldsymbol{I}) N_j dV \, \ddot{\boldsymbol{q}}_{sj} \tag{34}$$

where $\ddot{\boldsymbol{q}}$ is the nodal acceleration vector and $\boldsymbol{I}$ is

$$\boldsymbol{I} = \begin{bmatrix} 1 & 0 & 0 & 0 \\ 0 & 1 & 0 & 0 \\ 0 & 0 & 1 & 0 \\ 0 & 0 & 0 & 0 \end{bmatrix} \tag{35}$$

The last equation can be rewritten in the following compact manner

$$\delta L_{ine} = \delta \boldsymbol{q}_{\tau i}^T \boldsymbol{M}^{ij\tau s} \ddot{\boldsymbol{q}}_{sj} \tag{36}$$

where $\boldsymbol{M}^{ij\tau s}$ is the mass matrix in the form of the fundamental nucleus. The dimension of the array is $4x4$.The non-zero components of the matrix are

$$M_{11}^{ij\tau s} = M_{22}^{ij\tau s} = M_{33}^{ij\tau s} = \rho \int_{\Omega} F_{\tau} F_s dx dz \int_l N_i N_j dy \tag{37}$$

The fourth term of the matrix diagonal is zero, because the electrical part is neglected in the mass matrix.

The undamped dynamic problem can be written as follows
$$\boldsymbol{M}\ddot{\boldsymbol{a}} + \boldsymbol{K}\boldsymbol{a} = \boldsymbol{p} \tag{38}$$

where $\boldsymbol{a}$ is the vector of the nodal unknowns and $\boldsymbol{p}$ is the loading vector. By introducing harmonic solutions,it is possible to compute the natural frequencies, ω_i , for the homogenous case, by solving an eigenvalueproblem

$$\left(-\omega_i^2 \boldsymbol{M} + \boldsymbol{K}\right)\boldsymbol{a}_i = 0 \tag{39}$$

where $\boldsymbol{a}_i$ is the i−th eigenvector.

3.2 Loading vector

The loading vector that is variationally coherent to the model, in the case of a generic concentrated load $\boldsymbol{P}$, is

$$\boldsymbol{P} = \{P_{ux} P_{uy} P_{uz} 0\} \tag{40}$$

The virtual work due to $\boldsymbol{P}$ is
$$\delta L_{ext} = \boldsymbol{P}\delta \boldsymbol{u}^T \tag{41}$$

The virtual variation of $\boldsymbol{u}$ in the framework of CUF is
$$\delta L_{ext} = F_{\tau} \boldsymbol{P}\delta \boldsymbol{u}_{\tau}^T \tag{42}$$

By introducing the nodal displacements and the shape functions, the previous equation becomes

$$\delta L_{ext} = F_{\tau} N_i \boldsymbol{P}\delta \boldsymbol{u}_{\tau i}^T \tag{43}$$

4. Results and discussion

The aim of this section is to provide numerical examples in order to highlight the enhanced capabilities of the present 1D electro-mechanical formulation. Both actuator and sensor cases have been studied.

4.1 Polyvinylidene (PVDF) bimorph beam.

A cantilever beam, consisting of two PVDF layers with opposite polarities is considered. The total height or thickness is 0.001 m, the length is 0.1 m and the width is 0.005 m. The cantilever is fixed to the left end and an electric potential of 1 V is applied across the thickness. The relevant data are shown in Table 4. The cantilever bimorph PVDF model does not include the e33 and e15 piezoelectric constants. The geometry of the beam is reported in Fig. 6. The numerical results obtained with the present method are compared with results from other methods in Table 5. Valey and Rao (1994) used a 2D plane stress element modified with pseudo-nodes to include the electric potential DOF. Tzou and Ye (1996) adopted triangular shell elements with both mechanical (FOSDT) and electrical DOFs. Chee *et al*. (1999) used Hermitian beam elements with electric potential incorporated via a layer-wise formulation. Hwang and Park (1993) used a classical displacement field with five plate elements for the same problem. Separate actuator and sensor equations were used to calculate the control forces for actuation and to calculate charges for sensing that were not incorporated in their FE analysis. The results of the deflection of the cantilever bimorph along the length (same model as above) using the present method are compared with the results of Hwang and Park (1993) (including Tseng's data) in Fig. 7. The effect of varying the input actuation voltage (0-200 V) is reported in Fig. 8. The results agree to a great extent with those of Hwang and Park (1993) and of Tzou and Tsegn (1990). Fig. 9 shows the total voltage difference across the PVDF bimorph cantilever plotted along the length of the cantilever when the bimorph acts as a sensor. A vertical tip displacement of 1 cm is imposed. This case is implemented in the same way as the actuator case, except for the electrical boundary conditions. The Hwang and Park (1993), Tzou and Tsegn (1990) and Chee *et al*. (1999) results are also reported in the same figure. In the Hwang and Park model, there are five separate electrodes that cover the entire length of the beam. Each electrode, being an equipotential surface, must have a constant voltage, and this leads to the step distribution shown in Fig. 9. The results show that the present formulation offers results that are in good agreement with the results from the bibliography.

Table 3 L9 cross-section element point natural coordinates

Points	r	s
1	-1	-1
2	0	-1
3	1	-1
4	1	0
5	1	1
6	0	1
7	-1	1
8	-1	0
9	0	0

Table 4 Properties of the bimorph cantilever beam

	PVDF	
Elastic modulus	2.00×10^9	Pa
Shear modulus	7.75×10^8	Pa
Mass density	1.80×10^3	Kgm^{-3}
Poisson's ratio	0.29	--
e_{31}	0.046	Cm^{-2}
e_{32}	0.046	Cm^{-2}
χ_{11}	1.06×10^{-10}	Fm^{-1}
χ_{22}	1.06×10^{-10}	Fm^{-1}
χ_{33}	1.06×10^{-10}	Fm^{-1}
L length	0.1	m
h height	0.001	m
b width	0.005	m

Table 5 Deflections along the length of the beam, 1V

| Position	Chee *et al.* (1999)	Theory-Tzou and Ye (1996)	FEM-Valey and Rao (1994)	Solid FE-Tzou and Ye (1996)	Shell FE-Tzou and Ye (1996)	CUF 1D
m	w(m)	w(m)	w(m)	w(m)	w(m)	w(m)
0.00	0.000	0.000	0.000	0.000	0.000	0.000
0.02	1.380×10^{-8}	1.380×10^{-8}	1.380×10^{-8}	1.240×10^{-8}	1.32×10^{-8}	1.316×10^{-8}
0.04	5.520×10^{-8}	5.520×10^{-8}	5.520×10^{-8}	5.08×10^{-8}	5.280×10^{-8}	5.266×10^{-8}
0.06	1.424×10^{-7}	1.424×10^{-7}	1.424×10^{-7}	1.16×10^{-7}	1.190×10^{-7}	1.185×10^{-7}
0.08	2.208×10^{-7}	2.210×10^{-7}	2.210×10^{-7}	2.10×10^{-7}	2.110×10^{-7}	2.106×10^{-7}
0.10	3.450×10^{-7}	3.450×10^{-7}	3.450×10^{-7}	3.30×10^{-7}	3.300×10^{-7}	3.292×10^{-7}
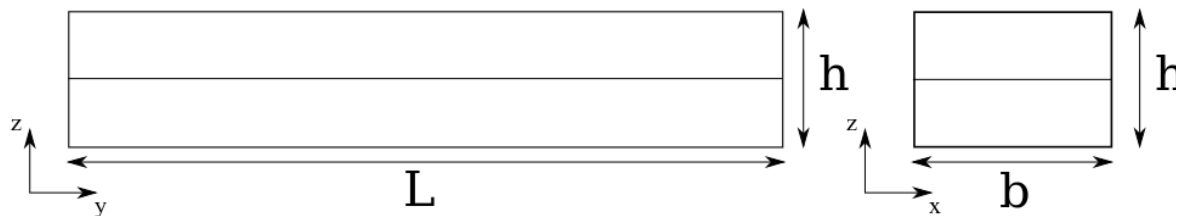
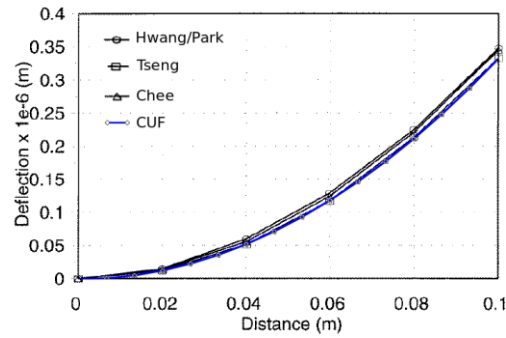Fig. 6 Geometry of the bimorph cantilever beam

Fig. 7 Actuator configuration. Deflection of the bimorph cantilever along its length
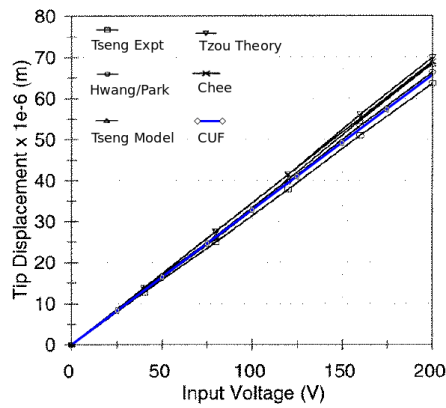

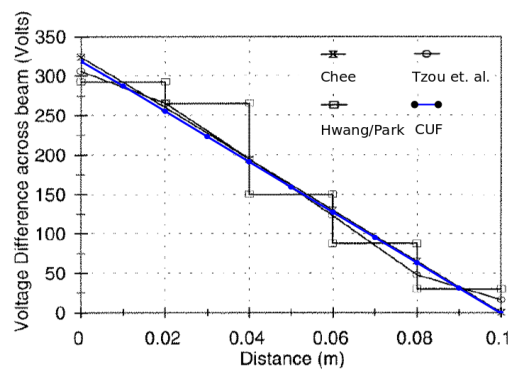Fig. 8 Actuator configuration. Tip deflection of the bimorph cantilever as a function of input actuator voltage

Fig. 9 Sensor configuration. Voltage difference across thickness of PVDF at various points along the length of the cantilever

4.2 Three-layer active cantilever.

This three-layer cantilever structure, which was studied by Sarvanos and Heyliger (1995), consists of a substrate (bottom layer), an adhesive (middle layer) and a piezoelectric material (top layer). The piezoelectric layer acts as an actuator which has an applied voltage difference of 12.5 kV across the thickness direction (Saravanos and Heyliger used a similar high voltage in order to compare their results with those of Robbins and Reddy (1991b) who applied an induced strain actuation of 0.1%). The substrate is made of isotropic aluminum or a Gr/epoxy composite T300/934. The material properties and the relevant data are shown in Table 6. The geometry of the beam is reported in Fig. 10. The length and width of the three layers are the same but the thickness of the substrate and piezoelectric are 1/10 and 1/100 of the length, respectively. The results are shown in Fig. 11 together with the results obtained by Sarvanos and Heyliger (1995) and Chee *et al*. (1999). It is possible to see that the CUF formulation is able to reproduce the same results of 11, Sarvanos and Heyliger (1995) and Chee *et al*. (1999).

The sensory capability is also investigated. The electric potential at the top and the bottom surfaces of the piezoelectric material were taken as free/sensing variables. An upward load of 1000 N was applied to the cantilever tip. Due to the electro-mechanical coupling, charges were generated on the piezoelectric material that resulted in a potential difference. The mid-plane deflections along the beam and the total voltage across the thickness of the piezoelectric are plotted in Figs. 12 and 13, respectively, together with the results obtained by Sarvanos and Heyliger (1995) and Chee *et al*. (1999). It is possible to see that the present formulation show an excellent agreement with the results from bibliography.

Table 6 Properties of the three-layer cantilever (data retried from Sarvanos and Heyliger (1995), Sarvanos(1997))

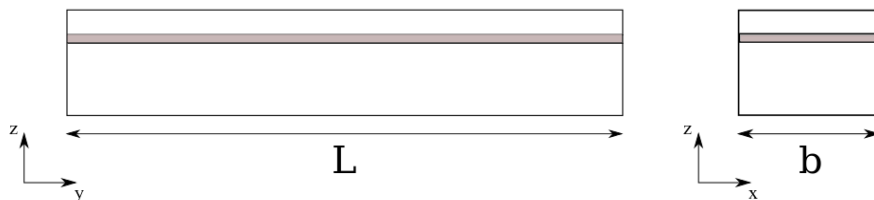|	Aluminium	T300/934	Adhesive	PZT-4	
E_{33}	6.8900×10^{10}	1.3238×10^{11}	6.9000×10^{9}	8.1300×10^{10}	Pa
E_{11}	6.8900×10^{10}	1.0760×10^{10}	6.9000×10^{9}	6.4500×10^{10}	Pa
v_{13}	0.25	0.24	0.4	0.43	-
G_{13}	2.7600×10^{10}	5.6500×10^{9}	2.4600×10^{9}	2.5600×10^{10}	Pa
d_{32}	-	-	-	-1.22×10^{-10}	m/V
χ_{22}	-	3.0989×10^{-11}	-	1.3059×10^{-8}	F/m
χ_{33}	-	2.6562×10^{-11}	-	1.1510×10^{-8}	F/m
L	0.1524	0.1524	0.1524	0.1524	m
h	0.01524	0.01524	0.000254	0.001524	m
b	0.0254	0.0254	0.0254	0.0254	m

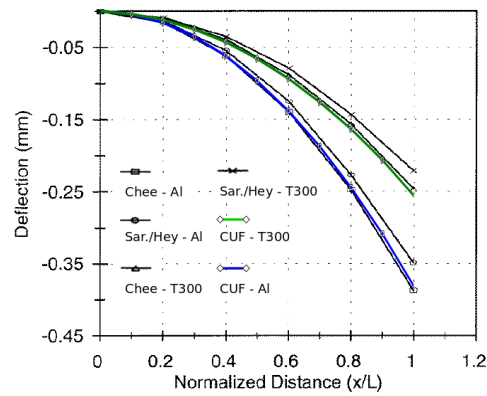Fig. 10 Three-layer actuator/sensor cantilever beam

Fig. 11 Actuator configuration. Deflection by piezoelectric actuation along the normalized length of the cantilever
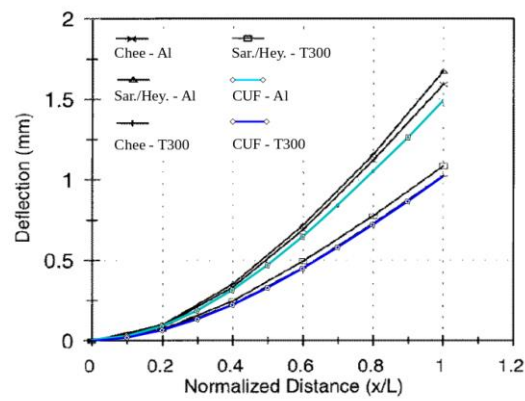

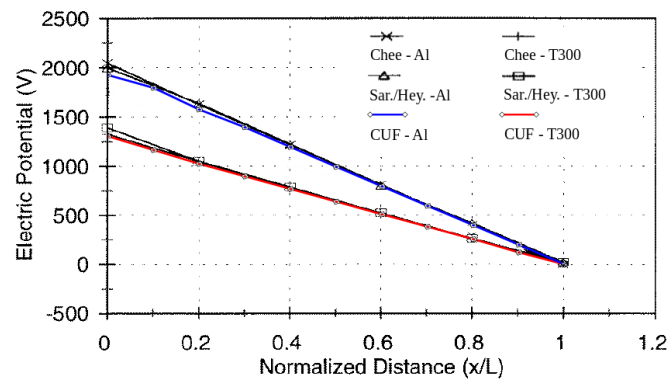Fig. 12 Sensor configuration. Deflection due to a load at the cantilever tip

Fig. 13 Sensor configuration. Voltage difference across the piezoelectric material v.s. the normalized length of the cantilever

4.3 Aluminum cantilever beam with two thin piezo-ceramic PSI-5A-S3 sheets

An aluminium beam with two thin piezo-ceramic sheets Yocum and Abramovich (2002) is studied. Thematerial property and the geometry of the beam are reported in Table 7 and Fig. 14. A comparison of the experimental and ADINA results obtained from the work of Yocum and Abramovich (2002) and the present model is reported in Figs. 15 and 16. Fig. 15 report the case for one piezo-actuator activated while Fig. 16reports the case for both pieo-actuators activated.

The results show that:
- the present model is able to give the same results as the ADINA commercial code;
- the present model is able to detect the experimental results;
- through the present 1D formulation, it is possible to study beams with variable and non-homogeneouscross-sections.
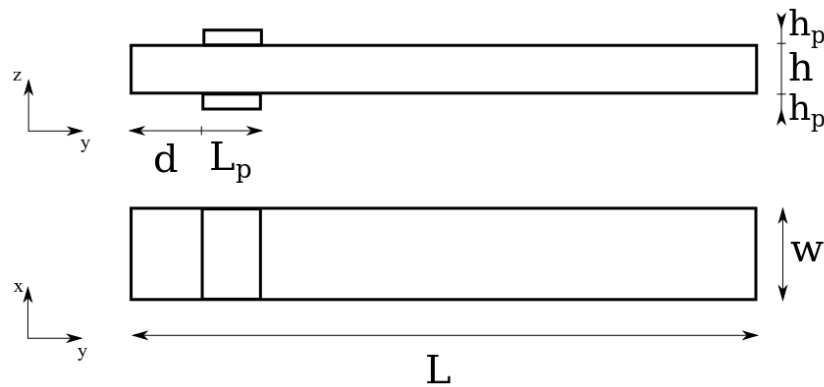

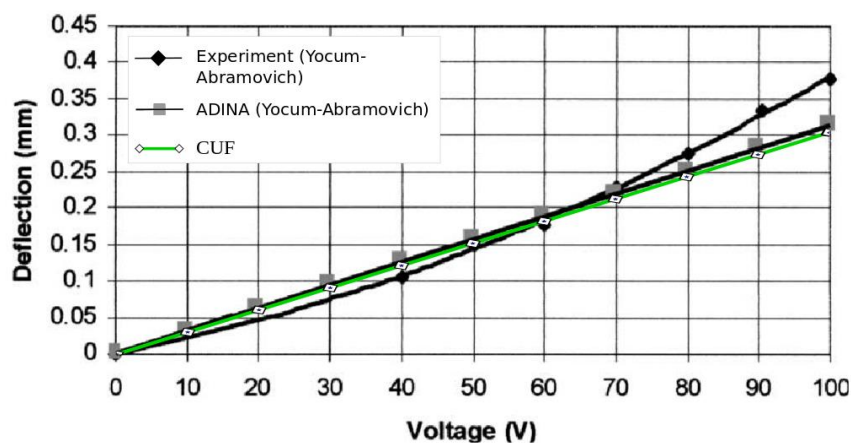Fig. 14 Geometry of a cantilever beam with two thin piezoceramic PSI-5A-S3 sheets

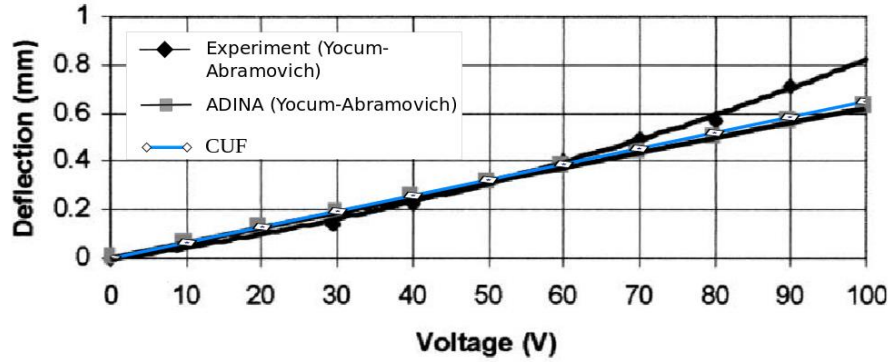Fig. 15 Deflection vs applied voltage, one piezo-patch activated

Fig. 16 Deflection vs applied voltage, two piezo-patchs activated

Table 7 Properties of the cantilever beam with two thin piezoceramic PSI-5A-S3 sheets

	Piezo	
Composition	Single sheet 5A-S3 (PZT)	-
Thickness	0.191 ± 0.013	mm
Length	54.5	mm
Width	54.5	mm
Distance from clamped side	30.0	mm
	Beam	
Composition	Aluminium	-
Thickness	1.6	mm
Length	356	mm
Width	54.5	mm

4.4 Piezoelectric plate

A plate composed of two identical piezoelectric layers is considered. The two layers are bonded perfectly to each other, with electrodes at the interface and on the upper and lower sides of the plate. The electrode at the interface is grounded. The material parameters and the plate geometry are reported in Table 7. A modal analysis has been performed for different mechanical boundary conditions and electrical boundary conditions. The results, compared with those of (Krommer (2003)), are reported in Tables 9-11. while Figs. 18-20 report the ratios between the natural frequencies obtained with the coupled formulations and the purely elastic ones

$$r = \frac{f_C}{f_N} \tag{44}$$

where f_C is the natural frequency obtained with the coupled formulation and f_N is natural frequency in thepurely elastic formulation. It is possible to see that the present model obtains an excellent agreement withthe results of Krommer (2003). The results show that the present 1D formulation is able to give the same result of a bi-dimensional formulation.

A rectangular aluminium cantilever plate with four rectangular PZT patches, bonded to the top surface of the plate and four other PZT patches bonded symmetrically to the bottom surface is

considered The configuration is depicted in Fig. 21. The material properties and geometrical dimensions of the plate and PZT layers are listed in Table 12. The modal analysis has been performed for two cases and the results have been compared with those of Yasin *et al.* (2010). In case 1, the piezoelectric patches are short-circuited, thereby making the piezoelectric coupling effect that enhances the stiffness of otherwise passive structure ineffective. Since the patches are short circuited, no electrical potential will build up across them, due to deformation that reduces the coupling terms to zero. In case 2, all 8 PZT patches act as sensors. The lowest seven natural frequencies for the cantilever plate in the two different cases are reported in Table 13. The table also reports the frequencies computed byYasin *et al.* (2010). The first four modes of the plate are reported in Fig. 22. It can be observed that both the obtained results are in excellent agreement with those presented in the reference.
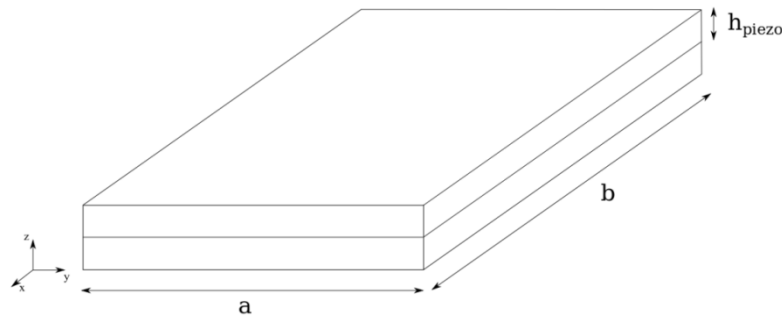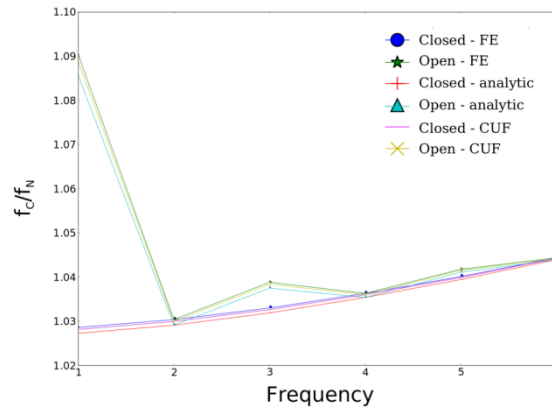

Fig. 17 Piezoelectric plate

Fig. 18 Natural frequency ratio between electro-mechanically coupled natural frequencies f_C andelastic natural frequencies f_N for an hinged-hinged panel. Analytical and FE results were taken fromKrommer (2003)

Fig. 19 Natural frequency ratio between electro-mechanically coupled natural frequencies f_C and elastic natural frequencies f_N for a clamped-hinged panel. Analytical and FE results were taken from Krommer (2003)
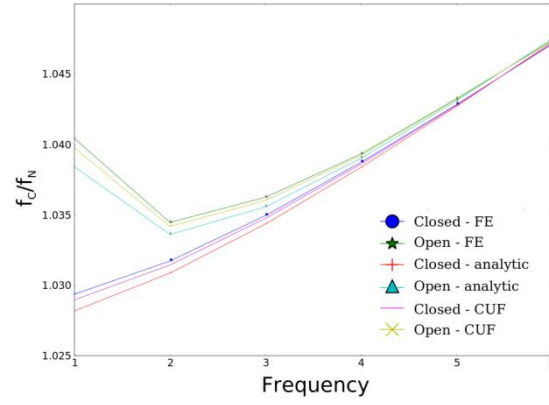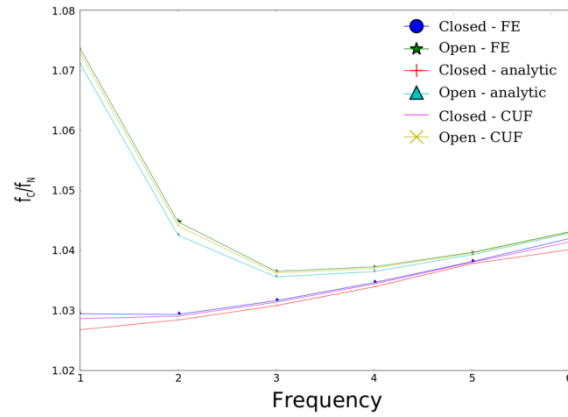

Fig. 20 Natural frequency ratio between electro-mechanically coupled natural frequencies f_C and elasticnatural frequencies f_N for a clamped-free panel. Analytical and FE results were taken from Krommer (2003)

According to the results it is possible to underline that

• the electro-mechanical effects in the modal analyses are correctly detected;
• the present formulation is able to give the same results of a bi-dimensional model;
• complex plate configurations can be studied, in particular, the patches can be locally distributed along the structure
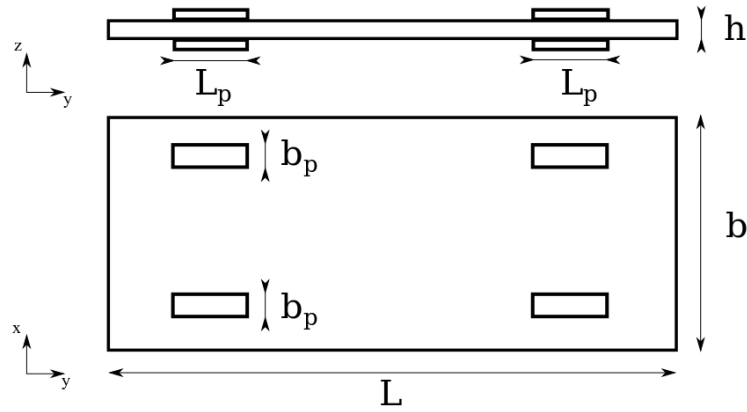
Fig. 21 Actuated plate

Table 8 Bi-morph plate properties

a	1	m
b	1	m
h_{piezo}	0.05	m
PZT-5A		
C_{22}	121×10^9	Pa
C_{33}	121×10^9	Pa
C_{11}	111×10^9	Pa
C_{23}	75.4×10^9	Pa
C_{21}	75.2×10^9	Pa
C_{31}	75.2×10^9	Pa
C_{44}	21.8×10^9	Pa
C_{55}	21.8×10^9	Pa
C_{66}	22.8×10^9	Pa
e_{31}	-5.46	Cm^{-2}
e_{32}	-5.46	Cm^{-2}
e_{33}	15.8	Cm^{-2}
e_{15}	12.32	Cm^{-2}
e_{24}	12.32	Cm^{-2}
χ_{11}	$1730\chi_0$	$AsV^{-1}m^{-1}$
χ_{22}	$1730\chi_0$	$AsV^{-1}m^{-1}$
χ_{33}	$1700\chi_0$	$AsV^{-1}m^{-1}$
ρ	7750	kgm^{-1}
$\chi_0 = 8.854 \times 10^{-12}$ $AsV^{-1}m^{-1}$		

  Not reported values are equal to zero

Table 9 Natural frequencies of the hinged-hinged panel ($rad\ s^{-1}$) - analytical and FE results were obtained from Krommer (2003)

|	1st	2nd	3rd	4th	5th	6th
Elastic/FE	864.4	3276.0	6830.9	11130	15880	20891
Elastic/analytic	840.1	3186.6	6650.6	10844.5	15481.8	20376.8
Elastic/CUF	813.0	3142.0	6612.9	10844.3	15553.2	20555.8
Closed/FE	889.1	3375.5	7056.3	11534	16517	21818
Closed/analytic	863.0	3279.3	6862.6	1128.1	16092.4	21271.9
Closed/CUF	835.9	3236.2	6828.6	11234.6	16173.6	21464.8
Open/FE	942.5	3375.5	7096.1	11534	16543	21818
Open/analytic	912.0	3279.3	6900.1	1128.1	16118.2	21271.9
Open/CUF	885.21	3236.1	6866.7	11234.6	16199.2	21464.8

Table 10 Natural frequencies of the clamped-hinged panel ($rad\ s^{-1}$)- analytical and FE results were obtained from Krommer (2003)

	1st	2nd	3rd	4th	5th	6th
Elastic/FE	1318.0	3977.4	7610.9	11871	16523	21420
Elastic/analytic	1244.8	3864.2	7407.5	11568.3	16114.7	20899.7
Elastic/CUF	1264.7	3855.7	7429.2	11646.4	16276.5	20230.5
Closed/FE	1356.7	4103.6	7877	12331	17231	22430
Closed/analytic	1313.8	3983.5	7662.0	12012.4	16803.3	21888.1
Closed/CUF	1301.4	3976.9	7687.5	12096.3	16973.3	21185.3
Open/FE	1371.3	4114.5	7886.9	12338	17238	22435
Open/analytic	1326.9	3994.1	7671.0	12019.8	16809.5	21893.2
Open/CUF	1315.0	3987.5	7696.9	12103.3	16980.0	21190.1

Table 11 Natural frequencies of the clamped-free panel ($rad\ s^{-1}$) - analytical and FE results were obtained from Krommer (2003)

|	1st	2nd	3rd	4th	5th	6th
Elastic/FE	312.4	1854.1	4822.5	8648.4	13035	17765
Elastic/analytic	302.3	1798.5	4687.6	8421.4	12708.6	17334.8
Elastic/CUF	299.4	1731.3	4731.2	8442.5	12763.9	17250.4
Closed/FE	321.2	1980.8	4975.0	9847.9	13532	18511
Closed/analytic	310.4	1849.6	4832.0	8708.1	13188.8	18060.4
Closed/CUF	308.0	1781.6	4879.6	8732.8	13249.1	17964.0
Open/FE	335.4	1937.1	4998.6	8970.7	13552	18531
Open/analytic	323.8	1875.0	4854.4	8728.6	13207.7	18078.1
Open/CUF	321.2	1807.5	4902.5	8754.9	13268.5	17992.8

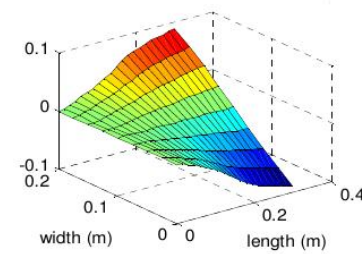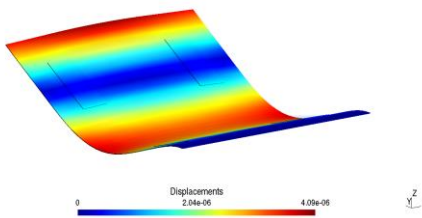*F. Miglioretti, E. Carrera and M. Petrolo*
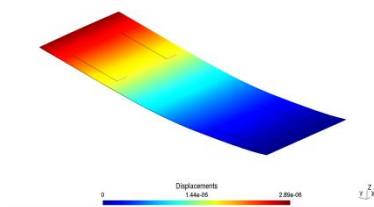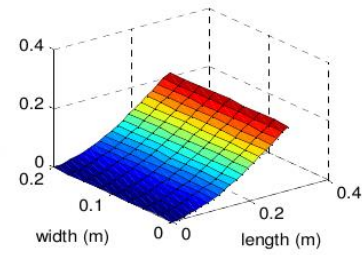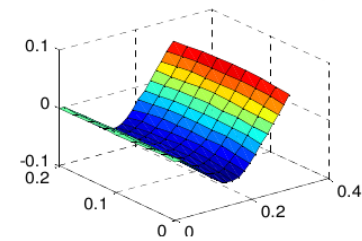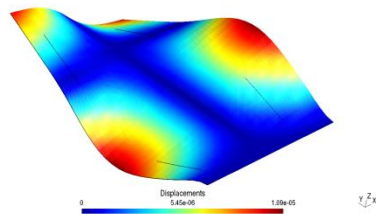

(a) First mode CUF.

(b) First mode Yasin et al.(2010).
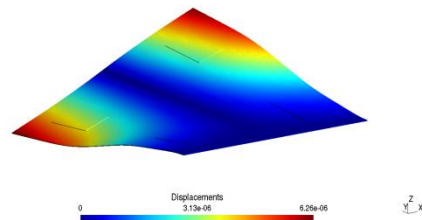
(c) Second mode CUF.

(d) Second mode Yasin *et al*. (2010).

(e) Third mode CUF.

(f) Third mode Yasin *et al*. (2010).
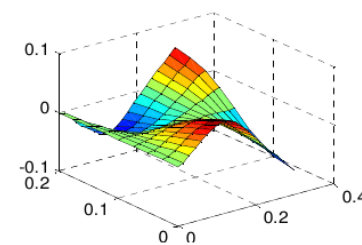

(g) Fourth mode CUF.

(h) Fourth mode Yasin *et al*. (2010).

Fig. 22 First four modes of the actuated plate

Table 12 Actuated plate properties

	Actuator	
$E_1 = E_2 = E_3$	$63 \ x \ 10^9$	Pa
$G_{12} = G_{13} = G_{23}$	$24.8 \ x \ 10^9$	Pa
ρ	$7.6 \ x \ 10^3$	Kgm^{-3}
ν	0.28	-
$d_{31} = d_{32}$	-220	pmV^{-1}
d_{33}	374	pmV^{-1}
$d_{24} = d_{15}$	670	pmV^{-1}
χ_{11}	$15.3 \ x \ 10^{-9}$	Fm^{-1}
χ_{22}	$15.3 \ x \ 10^{-9}$	Fm^{-1}
χ_{33}	$15.0 \ x \ 10^{-9}$	Fm^{-1}
L	0.06	m
h	$0.63 \ x \ 10^{-3}$	m
b	0.025	m
	Plate	
E	$70 \ x \ 10^9$	Pa
ρ	$2.7 \ x \ 10^3$	Kgm^{-3}
ν	0.33	-
L	0.3	m
h	$0.8 \ x \ 10^{-3}$	m
b	0.2	m

Table 13 First eight natural frequencies of the plate

	CUF(Hz)	CUF(Hz)	Yasin *et al.*(2010) (Hz)	Yasin *et al.*(2010) (Hz)
	Case 1	Case 2	Case 1	Case 2
1	7.4986	7.5685	7.5236	7.5639
2	25.391	25.422	25.195	25.221
3	46.154	46.187	45.542	45.591
4	94.451	94.580	90.215	90.371
5	124.30	124.43	123.03	123.10
6	180.78	181.82	183.16	185.11
7	245.59	245.72	234.05	234.05

Case 1 : piezoelectric patches are short circuited.

Case 2 : all eight piezoelectric patches are acting as sensors (open).

5. Conclusions

The hierarchical capabilities of CUF have been exploited in this paper to develop 1D FE based on polynomial expansions of the cross-section unknowns. It is important to underline that the choice of the expansion and its order are arbitrary since CUF models are based on the so-called fundamental nucleus assembly methodology which allows one to use any-order models and different classes with no need for formal changes in the problem equations. Different test cases

have been exploited in order to evaluate the capabilities of the present formulation. Three different cantilever beams have been studied in the actuator and sensor configuration. Static results have been collected and compared with results from bibliography. The first case was a PVDF bimorph cantilever beam while the second case was a three-layer cantilever beam. The two cases show a distributed piezo layer along the length of the beam. Piezoelectric patches have been studied in the third case, where a cantilever metallic beam with two piezo-patches has been studied. Two different plates have been also considered. A bimorph plate and a metallic plate with eight piezoelectric patches have been studied. Dynamic analyses have been performed and the results compared with those from bibliography.

The main conclusions are the following:

- the present formulation is able to correctly detect electro-mechanical interaction;
- the present formulation is able to study beams with variable and non-homogeneous cross-section;
- through the present 1D-formulation, it is possible to study typical plate problems via beam models.
- in particular, piezoelectric patches can be locally inserted along the structure.

In future extension a response model could be implemented, in order to study the transient influence of different electrical boundary conditions.

References

Bailey, T. and Hubbard, J. (1985), "Distributed piezoelectric polymer active vibration control of a cantilever beam", *AIAA J.*, **8**(5), 605-611.

Ballhause, D., D'Ottavio, M., Kroplin, B. and Carrera, E. (2005), "A unified formulation to assess multilayered theories for piezoelectric plates", *Comput. Struct.*, **83**(15-16), 1217-1235.

Bathe, K. (1996), *Finite element procedure*, Prentice hall.

Beheshti-Aval, S., Lezgy-Nazargah, M., Vidal, P. and Polit, O. (2011), "A refined sinusfinite element model for the analysis of piezoelectric-laminated beams", *J. Intel. Mat. Syst. Str.*, **22**(3), 203-210.

Biscani, F., Nali, P., Belouettar, S. and Carrera, E. (2012), "Coupling of hierarchical piezo-electric plate finite elements via arlequin method", *J. Intel. Mat. Syst. Str.*, **23**(7), 749-764.

Carrera, E. (1997), "An improved Reissner-Mindlin-Type model for the electromechanical analysis of multilayered plates including piezo-layers" *J. Intel. Mat. Syst. Str.*, **8**(3)232-248.

Carrera, E. and Boscolo, M. (2006), "Classical and mixed finite elements for static and dynamic analysis of piezoelectric plates", *Int. J. Numer. Meth. Eng.*, **70**(10), 1135-1181.

Carrera, E. and Giunta, G. (2010), "Refined beam theories based on a unified formulation", *Int. J. Appl. Mech.*, **2**(1), 117-143.

Carrera, E., Giunta, G., Nali, P. and Petrolo, M. (2010), "Refined beam elements with arbitrary cross-section geometries", *Comput. Struct.*, **88**(5-6), 283-293.

Carrera, E. and Petrolo, M. (2011), "On the effectiveness of higher-order terms in refined beam theories", *J. Appl. Mech. - T ASME*, 7 (2), 021013, doi:10.1115/1.4002207.

Carrera, E., Biscretto, S. and Nali, P. (2011), *Plates and shells for smart structures*, John Wiley and sons.

Carrera, E. and Petrolo, M. (2012), "Refined beam elements with only displacement variables and plate/shell capabilities", *Meccanica*, **47**(3), 537-556.

Carrera, E., Petrolo, M. and Nali, P. (2011), "Unified formulation applied to free vibrations finite element analysis of beams with arbitrary section", *Shock Vib.*, **18**(3), 485-502.

Carrera, E., Petrolo, M. and Varello, A. (2012a), "Advanced beam formulations for free vibrations analysis of conventional and joined wings", *J. Aerospace Eng.*, **25**(2), 282-293.

Carrera, E., Zappino, E. and Petrolo, M. (2012b), "Advanced elements for the static analysis of beams with compact and bridge-like sections", *J. Struct. Eng. - ASCE*, **56**, 49-61.

Caruso, G., Galeani, S. and Menini, L. (2003), "Active vibration control of an elastic plate using multiple piezoelectric sensors and actuators", *Simul. Model. Pract. Th.*, **11**(5-6), 403-419.

Chee, C., Tong, L. and Steven, G. (1999), "A mixed model for composite beams with piezoelectric actuators and sensors", *Smart Mater. Struct.*, **8**(3), 417, doi:10.1088/0964-1726/8/3/313.

Crawley, E. and Luis, J. (1987), "Use of piezoelectric actuators as elements of intelligent structures", *AIAA J.*, **25**(10), 1373-1385.

Dong, X.J., Meng, G. and Peng, J.C. (2006), "Vibration control of piezoelectric actuators smart structures based on system identification technique: numerical simulation and experimental study", *J. Sound Vib.*, **297**(3-5), 680-693.

Elshafei, M. and Alraiess, F. (2013), "Modeling and analysis of smart piezoelectric beams using simple higher order shear deformation theory", *Smart Mater. Struct.*, **22**(3), doi:10.1088/0964-1726/22/3/035006.

Hwang, W. and Park, H. (1993), "Finite element modelling of piezoelectric sensors and actuators", *AIAA J.*, **31**(5), 930-937.

Kim, T.W. and Kim, J.H. (2005), "Optimal distribution of an active layer for transient vibration control of an flexible plates", *Smart Mater. Struct.*, **14**(5), 904-916.

Krommer, M. (2003), "Piezoelestic vibrations of composite Reissner-Mindlin-type plates", *J. Sound Vib.*, **263**(4), 871-891.

Kumar, K. and Narayanan, S. (2007), "The optimal location of piezolectric actuators and sensors for vibration controls of plate", *Smart Mater. Struct.*, **16**(6), 2680-2691.

Kusculuoglu, Z.K. and Royston, T.J. (2005), "Finite element formulation for composite plates with piezoceramic layers for optimal vibration control applications", *Smart Mater. Struct.*, **14**(6), 1139-1153.

Liu, G., Dai, K. and Lim, K. (2004), "Static and vibration control of composite laminates integrated with piezoelectric sensors and actuators using radial point interpolation method", *Smart Mater. Struct.*, **13**(6), 1438-1447.

Marinkovic, D., Koppe, H. and Gabber, H. (2007), "Accurate modelling of the electric field within piezoelectric layers for active composite structures", *J. Intel. Mat. Syst. Str.*, **18**(5), 503-513.

Moita, J., Soares, C. and Soares, C. (2005), "Active control of forced vibration in adaptive structures using a higher order model", *Compos. Struct.*, **71**(3-4), 349-355.

Moitha, J., Correira, I., Soares, C. and Soares, C. (2004), "Active control of adaptive laminated structures with bonded piezoelectric sensors and actuators", *Comput. Struct.*, **82**(17-19), 1349-1358.

Onate, E. (2009), *Structural analysis with the finite element method: linear statics*, Springer.

Robbins, D. and Reddy, J. (1991a), "Analysis of piezoelectrically actuated beam using a layer-wise displacements theory", *Comput. Struct.*, **41**(2), 265-279.

Robbins, D. and Reddy, J. (1991b), "Analysis of piezoelectrically actuated beams using a layer-wise displacement theory", *Comput. Struct.*, **41**(2), 265-279.

Sarvanos, D. and Heyliger, P. (1995), "Coupled layer wise analysis of composite beams with embedded piezoelectric sensors and actuators", *J. Intel. Mat. Syst. Str.*, **6**(3), 350-363.

Sarvanos, D. and Heyliger, P. (1999), "Mechanics and computational models for laminated piezoelectric beams, plate, and shells", *Appl. Mech. Rev.*, **52**(10), 305-320.

Sarvanos, D.A. (1997), "Mixed laminate theory and finite element for smart piezoelectric composite shell structures", *AIAA J.*, **35**(8), 1327-1333.

Tzou, H. and Ye, R. (1996), "Analysis of piezoelastic structures with laminated piezoelectric triangle shell elements", *AIAA J.*, **34**(1), 110-115.

Tzou, H. and Tseng, C. (1990), "Distributed vibration control and identification of coupled elastic/piezoelectric systems: finite element formulation and applications", *Mech. Syst. Signal Pr.*, **5**(3), 215-231.

Umesh, K. and Ganguli, R. (2009), "Shape vibration control of smart plate with matrix cracks", *Smart Mater.*

Struct., **18**(2), 1-13.

Valey, D. and Rao, S. (1994), *Two-dimensional finite element modeling of composites with embedded piezoelectrics*, Collection Tech. Papers Proc. AIAA/ASME/ASCE/AHS/ASC Structures, Structural Dynamics and Materials Conf. 5, 2629-2633.

Vasques, C. and Rodrigues, J. (2006), "Active vibration of smart piezoelectric beams: comparison of classical and optimal feedback control strategies", *Comput. Struct.*, **84**(22-23),1459-1470.

Vidal, P., D'Ottavio, M., Thaier, M. and Polit, O. (2011), "An efficient finite shell element for the static resposne of piezoelectric laminates", *J. Intel. Mat. Syst. Struct.*, **22**(7),671.

Xu, S. and Koko, T. (2004), "Finite element analysis and design of actively a controlled piezoelectric smart structure", *Finite Elem. Anal. Des.*, **40**(3), 241-262.

Yasin, M.Y., Ahmad, N. and Alam, M.N. (2010), "Finite element analysis of actively controlled smart plate with patched actuators and sensors", *Latin Am. J. Solids Struct.*, **7**, 227-247.

Yocum, M. and Abramovich, H. (2002), "Static behaviour of piezoelectric actuated beams", *Comput. Struct.*, **80**(23), 1797-1808.

Zhou, X., Chattopadhyay, A. and Gu, H. (2000), "Dynamic response of smart composites using a coupled thermo-piezoelectric-mechanical model", *AIAA J.*, **38**(10), 1939-1948.

FC